



HAL
open science

The foreign-continuum absorption of water vapour in the far-infrared (50–500 cm⁻¹)

Aleksandra Koroleva, Tatyana Odintsova, Mikhail Yu. Tretyakov, Olivier Pirali, Alain Campargue

► **To cite this version:**

Aleksandra Koroleva, Tatyana Odintsova, Mikhail Yu. Tretyakov, Olivier Pirali, Alain Campargue. The foreign-continuum absorption of water vapour in the far-infrared (50–500 cm⁻¹). *Journal of Quantitative Spectroscopy and Radiative Transfer*, 2021, 261, pp.107486. 10.1016/j.jqsrt.2020.107486 . hal-03337025

HAL Id: hal-03337025

<https://hal.science/hal-03337025>

Submitted on 17 Nov 2021

HAL is a multi-disciplinary open access archive for the deposit and dissemination of scientific research documents, whether they are published or not. The documents may come from teaching and research institutions in France or abroad, or from public or private research centers.

L'archive ouverte pluridisciplinaire **HAL**, est destinée au dépôt et à la diffusion de documents scientifiques de niveau recherche, publiés ou non, émanant des établissements d'enseignement et de recherche français ou étrangers, des laboratoires publics ou privés.

Journal of Quantitative Spectroscopy and Radiative Transfer

The foreign-continuum absorption of water vapour in the far-infrared (50-500 cm⁻¹)

--Manuscript Draft--

Manuscript Number:	JQSRT_2020_468R2
Article Type:	VSI: HighRes-2019:Full Length Article
Keywords:	Terahertz gap; rotational spectrum; synchrotron; in-band continuum; Water vapour; bimolecular absorption
Corresponding Author:	alain Campargue cnrs Saint Martin d'Hères, France
First Author:	Aleksandra Koroleva
Order of Authors:	Aleksandra Koroleva Tatyana Odintsova Mikhail Tretyakov Olivier Pirali alain Campargue
Abstract:	The continuum absorption of water vapour diluted in nitrogen, oxygen and air is investigated in the range of the pure rotational band of the water molecule (50-500 cm ⁻¹). Spectra recordings were performed at room temperature with a Fourier transform spectrometer associated to a 151-m multipass gas cell located at the AILES beamline of SOLEIL synchrotron facility. The study includes the first laboratory measurements in the wide 90-330 cm ⁻¹ interval. Tests of the baseline stability, crucial for the continuum determination, are reported together with the expected pressure dependences of the continuum absorption, measured over different pressure ramps. Retrieved foreign-continuum cross-sections are found in good agreement with literature values available in the lower and upper parts of the studied frequency range. The reported results validate the MT_CKD foreign-continuum empirical model, widely used in atmospheric applications, even if some underestimation of the MT_CKD values is noted in the centre of the band.
Suggested Reviewers:	Andrey Vigasin vigasin@ifran.ru Igor Ptashnik piv@iao.ru manfred birk Manfred.birk@dlr.de Keith Shine k.p.shine@reading.ac.uk Eli Mlawer emlawer@aer.com Dave Tobin dave.tobin@ssec.wisc.edu
Response to Reviewers:	

Manuscript Number: JQSRT_2020_468R1

The foreign-continuum absorption of water vapour in the far-infrared (50-500 cm⁻¹)

We thank the reviewer for his/her comments. Most of his/her suggestions were taken into account as detailed below.

Editor and Reviewer comments:

Reviewer #1:

The revised version of this paper has clearly been improved, including the treatment of the dependence of the continuum on the widths. I provide here some points for the authors' consideration. Although I would welcome further modification of the paper to take these not-so-minor points into account, I recommend that the journal accept this manuscript (with minor revisions) even if the authors do not.

The Supplemental section has a very nice demonstration that the line list and continuum are inextricably linked, and the conclusion on page 9 about "systematic errors" is very apt. Based on the discussion on page 9, on lines 339-345, and in the "response to the reviewers", as well as the fairly low uncertainty values provided, the authors think that including in their continuum uncertainty budget the impact of their choice of using the HITRAN 2016 widths is not appropriate. That decision is consistent with previous continuum analyses, including the studies that are referenced on pages 12-13. In particular, Mlawer et al. (2019) does not directly consider in its uncertainty budget the difference in continuum coefficients that would have resulted from using the HITRAN 2012 widths instead of its derived values. Given the dramatic impact shown in Fig. S8, the dependence on widths clearly should have an impact on how readers think about the results of this study. The authors may want to consider a stronger statement about this consistency issue when presenting Fig. 8 and when using the words "agreement" or "overestimate".

*The good agreement with previous experimental studies is illustrated in Fig.8. We have also derived the continuum using the Mlawer2019 line list. So we are confident that the **overestimation** of the continuum by the MT_CKD model seen in Fig.8 is larger than could be explained by the differences in used line lists. We believe that our present statements are strong enough. However, the detailed comparison with the MT_CKD model will be included in a future publication and, so/hence/therefore we decided to omit our 5th highlight related to this issue "The MT_CKD model is validated in general, although some overestimation is noted"*

Perhaps the most important issue is what guidance a radiative transfer modeler who reads this paper should take with respect to the set of spectroscopic values they should use. It is probable that a modeler using HITRAN 2016 air-broadened widths would be wise to use the foreign continuum values in this study, while someone using the AER widths who uses these continuum values might not be making the best choice. In the response to reviewers, the authors make some points related to their choice of widths: "Note that Mlawer et al. widths (and intensities) are compiled on the basis of early HITRAN line lists. We believe that the use of more recent HITRAN data is preferable because of (i) permanent improvement of their general accuracy and completeness; (ii) easy accessibility by researchers and (iii) traceability of data. HITRAN error codes are used in the revised paper to assess associated uncertainty of the continuum." There are some points to make in reference to this:

- * The HITRAN 2012 widths used in the Mlawer et al. analysis in this region are the same widths as used in this study (HITRAN 2016); they originate from the same source. The intensities changed very little between the two versions.
- * Even if they weren't the same widths, the starting point for the width analysis in Mlawer et al. wouldn't be relevant since revised widths were derived and used.

* The width error codes in HITRAN are hard to take seriously, although it's hard to think of a better alternative to using them in the analysis the authors present in the Supplement.

* HITRAN 2020 is adopting the Mlawer et al. widths in this region. Based on the argument presented above, it would be questionable whether it would be wise for a modeler to use the foreign continuum values presented in this study with these new HITRAN widths. For this reason, the authors may want to consider switching to the HITRAN 2020 widths or providing foreign continuum coefficients derived with each width dataset (or, if possible, deriving their own widths from this experimental dataset).

The most important guidance a modeler should take is using a self-consistent set of parameters for the resonance lines and the continuum. It is underlined in lines 391-395, 441-443 of the manuscript and 261-264 of the Suppl.Mat. The continuum coefficients can be easily recalculated from one line list to another one from the total absorption using equations (1)-(5). Providing the continuum coefficients derived with different dataset is important for a modeler but it does not make sense for a general reader. Derivation of line widths from our experimental data is practically impossible. Such task requires special experimental campaign with the use of significantly different experimental method and conditions. We plan to implement this task in the future.

No modifications are made.

Minor comments:

82 - Remove the comma before "because"

corrected

112 - Should be "allow"

corrected

321-322 - It's hard to understand the phrase "evidencing about imperfect elimination of the baseline change by the correction term δ_{α} ", but its unclear meaning makes it difficult to suggest an alternate phrasing.

The sentence: "Periodic variations of the difference are seen for Series 3 and 4, evidencing about imperfect elimination of the baseline change by the correction term δ_{α} " is rephrase as follows:

"Periodic variations of the difference are seen for Series 3 and 4. These variations are similar to those shown in the lower part of Fig. S1. The similarity indicates an imperfect elimination of the baseline change by the correction term δ_{α} ".

396-399 - The parenthetical part of this sentence is hard to understand in its current location. Perhaps it should be moved earlier in the sentence to follow "resonance line list"? In addition, this parenthetical comment suggests that the Supplemental section analyzes the impact of using the widths from Mlawer et al. (2019) on the derived continuum, but those widths are not analyzed (or even mentioned) in the Supplement. A related small point: the reference provided for the AER widths is for the continuum, not the widths.

The unnecessary parenthetical part is removed.

439 – Planck

corrected

447 - "datasets" instead of "dataset"?

corrected

452 - I'm not sure "entails" is the word that was meant here. Maybe "affects" or "impacts"?
changed to "affects"

Supplemental

pg 6 - Is the consistency of the air- vs. N₂/O₂ broadened widths because the same source (e.g. Gamache) is used in each?

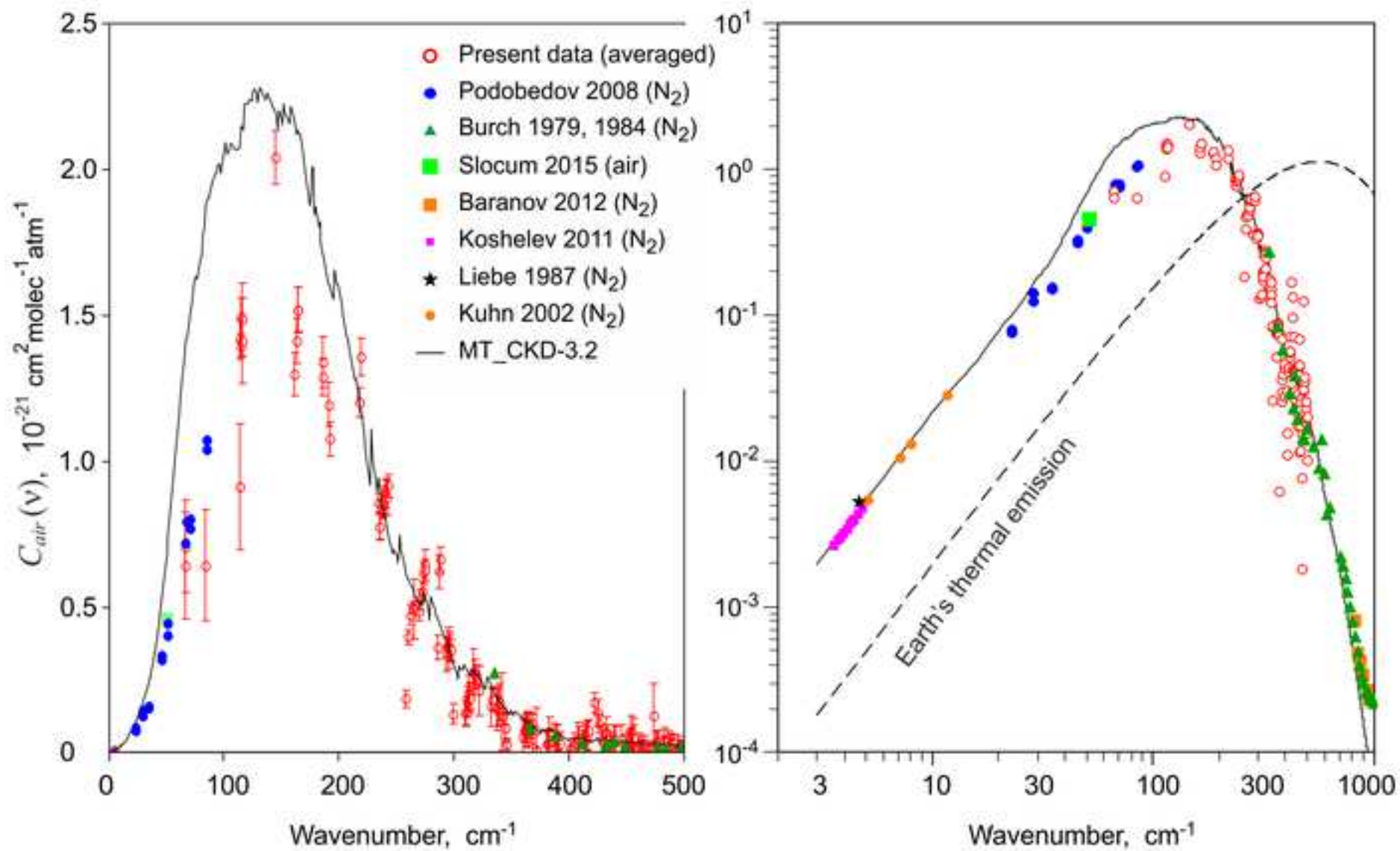
As far as we know, air, N₂ and O₂ widths are calculated on the basis of intermolecular interaction potential, which parameters are adjusted so the calculations reproduce the preselected (the most accurate) experimental data. So the primary sources are different experimental data. That is why the quantity $(0.79 \cdot \gamma_{N_2} + 0.21 \cdot \gamma_{O_2}) / \gamma_{air}$ is not exactly equal to unity (Fig. S7).

pg 7 - "A rough estimate of the impact of the monomer absorption can be obtained, however, by increasing or decreasing the broadening parameters of all lines simultaneously within the limits of their error bars." Are all the lines perturbed by the same percentage or different ones? if the former, can the uncertainty be provided; if the latter, can the average uncertainty be provided? This value would help put the results in Figure S8 in context.

The first question was answered in lines 222-223 of SupplMat: "...the impact was evaluated as the deviation of the continuum corresponding to maximum and minimum values of the broadening parameter within its stated uncertainty". The uncertainty is different for different lines. The range of the uncertainties and average is now mentioned in the text as follows: "...the impact was evaluated as deviation of the continuum corresponding to maximum and minimum values of the broadening parameter within its stated uncertainty (varying in the 1-20% range, near 19% on the average)..."

pg 8 - "could be quantify" should be "could be quantified".
corrected

- H₂O foreign-continuum absorption is retrieved at 296 K in the 50-500 cm⁻¹ range
- First laboratory measurements in the wide 90-330 cm⁻¹ interval including the range of maximum intensity of H₂O pure rotational band
- Expected pressure dependences of the continuum are verified
- The foreign-continuum cross-sections for O₂, N₂ and dry air are derived separately and used for data validation
- ~~The MT_CKD model is validated in general, although some overestimation is noted~~



31

Abstract

32 We investigated the continuum absorption of water vapour diluted in nitrogen, oxygen
33 and air in the range of the pure rotational band of the water molecule ($50\text{-}500\text{ cm}^{-1}$). Spectra
34 recordings were performed at room temperature with a Fourier transform spectrometer
35 associated to a 151-m multipass gas cell located at the AILES beamline of SOLEIL
36 synchrotron facility. The study includes the first laboratory measurements in the wide $90\text{-}330$
37 cm^{-1} interval. Tests of the baseline stability, crucial for the continuum determination, are
38 reported together with the expected pressure dependences of the continuum absorption,
39 measured over different pressure ramps. Retrieved foreign-continuum cross-sections are
40 found in good agreement with literature values available in the lower and upper parts of the
41 studied frequency range. The reported results validate the MT_CKD foreign-continuum
42 empirical model, widely used in atmospheric applications, even if some overestimation of the
43 MT_CKD values is noted in the centre of the band where experimental data were absent.
44

45 1. Introduction

46 Appropriate calculations of radiation balance, modelling of global climate changes, and
47 atmosphere remote sensing require an accurate quantification of atmospheric absorption in the
48 whole electromagnetic spectrum. The far-infrared region (usually defined as radiation within
49 frequency range of about 0.3 – 20 THz or 10 – 700 cm^{-1}) is of particular interest for
50 atmospheric sciences. The far-infrared (IR) region contains resonance lines of the major and
51 minor atmospheric constituents, such as O_2 , NO_2 , O_3 , NH_3 , CO_2 but water vapour, in spite of
52 its relatively small atmospheric abundance ($\sim 1\%$), is the dominant contributor to the
53 absorption of both incoming solar and outgoing thermal radiation [1-Clough1992, 2-
54 Harries2000, 3-Shine2012]. In the global average, the latter has maximum in the far IR range
55 near 560 cm^{-1} . In general, line parameters (centre frequency, intensity, pressure-shift and -
56 broadening coefficients) of these molecules as listed in current spectroscopic databases (*e.g.*
57 HITRAN [4-HITRAN2016]) are known and can be used in remote sensing experiments.

58 In addition to resonance lines, atmospheric absorption includes a weak non-resonant
59 continuum absorption (or just *continuum*), smoothly varying with frequency. Intermolecular
60 interactions during collisions are known as physical origin of the continuum. At atmospheric
61 conditions, pair interactions dominate over higher order effects (triple, quadruple, etc.) so the
62 continuum absorption can be considered as a result of bimolecular interactions.

63 Atmospheric continuum can be subdivided into a water-related component (wet
64 continuum) and a dry component (mostly due to the interaction of nitrogen and oxygen
65 molecules with each other). The wet continuum can be in turn divided into two contributions
66 corresponding to interaction of water molecules with each other (*self-continuum*) and with
67 other atmospheric molecules (*foreign-continuum*). It is known that the larger the dipole
68 moments of collisional partners (or the next term of multipole expansion of charge
69 distribution for non-polar molecules) are, the larger the continuum magnitude is. Water
70 molecule possesses dipole moment of 1.85 D that leads to a strong self-continuum.

71 Foreign water vapour continuum in air originates predominately from interaction of
72 H_2O molecules with the two most abundant atmospheric gases: nitrogen and oxygen. Being
73 symmetric diatomic molecules, neither O_2 nor N_2 possess an electric dipole moment. That is
74 why $\text{H}_2\text{O}-\text{N}_2$ and $\text{H}_2\text{O}-\text{O}_2$ foreign continuum cross-sections are significantly weaker than the
75 $\text{H}_2\text{O}-\text{H}_2\text{O}$ self-cross-sections. Nevertheless, in usual conditions, the high concentration of O_2
76 and N_2 makes both the foreign- and self-continua have an appreciable effect in the
77 atmosphere.

78 The wet continuum amplitude is very small compared to the absorption at the centre of
79 resonance lines. Nevertheless, due to its wide spectral extension, its contribution to the total
80 atmospheric absorption has significant impact on the greenhouse effect [3-Shine2012]. The
81 far IR dry air continuum component, corresponding mostly to interactions between O_2 and N_2
82 molecules can be generally neglected in normal and wet atmospheric conditions because the
83 corresponding bimolecular absorption cross-section is about one order of magnitude weaker
84 than H_2O foreign-continuum cross-section [5-Boissoles2003].

85 The continuum absorption is poorly studied in the far IR not only because of its
86 weakness, but also because of the well known difficulties of efficient generation and detection
87 of radiation in this spectral range, sometimes called the “THz gap” (see, *e.g.* review in [6-
88 Consolino2017]). The present contribution is part of a series of laboratory studies of the water
89 vapour continuum using synchrotron-based Fourier transform spectroscopy (FTS) technique.
90 The self-continuum absorption was first investigated in the 10-650 cm^{-1} range [7-
91 Odintsova2017, 8-Odintsova2019, 9-Odintsova2020]. This range covers most part of the H_2O
92 pure rotational band, thus the studied continuum can be classified as an *in-band* continuum.
93 The derived cross-sections together with the results of previous investigations by Burch (350-

94 800 cm^{-1}) [10-Burch1982] indicated that the MT_CKD model [11-Mlawer2012, 12-
95 Mlawer2019, 13-MTCKD_site], commonly used in radiative transfer codes, overestimates the
96 magnitude of the self-continuum in the considered range by about 30%. The present work is
97 devoted to a similar study and validation test of the MT_CKD foreign-continuum. Previous
98 laboratory measurements of the foreign-continuum were reported in the low- (3.5-84.1 cm^{-1})
99 [14-Koshelev2011, 15-Liebe1987, 16-Kuhn2002, 17-Podobedov2008-N2, 18-
100 Podobedov2008-O2] and high- (337.9-629.0 cm^{-1}) [19-Burch1979] frequency wings of the
101 H_2O band, missing the range where the band and the related continuum reach their maximum.
102 It should be mentioned, however, that foreign-continuum retrieval was performed over the
103 entire spectral range from atmospheric emitted (downwelling) spectral radiance observations
104 [20-Green2012, 21-Liuzzi2014, 22-Shi2016, 12-Mlawer2019]. These atmospheric
105 measurements are, on one hand, quite sensitive because of the long atmospheric path but on
106 the other hand, their accuracy is limited by uncertainties related to the atmospheric model and
107 poorly controlled environmental conditions. Nevertheless, these data provide the major
108 experimental constraints to the MT_CKD continuum coefficients in the far IR [12-
109 Mlawer2019].

110 The goal of the present work is thus a laboratory determination of the H_2O foreign-
111 continuum cross-sections associated with dry air, nitrogen and oxygen in the 50-500 cm^{-1}
112 frequency range. The measurements of O_2 - and N_2 -cross-sections **allow** us to check the
113 consistency with the separate determination of the air cross-sections. In Section 2, we give a
114 brief description of the experimental setup and spectra acquisition. The details of the data
115 analysis are given in Section 3. Section 4 presents the experimental results, their discussion
116 and comparison with previously known data. The conclusions are summarised in Section 5.
117 Additional information on the data analysis and the retrieved cross-section data are given in
118 *Supplementary Materials*.

119 2. Experimental set-up

120 The experimental approach is very similar to that used in [8-Odintsova2019]. The FTS
121 spectra of wet atmospheric gases (nitrogen, oxygen and dry air) were recorded at room
122 temperature (296 ± 1.5 K, permanently monitored by PT100 thermo-sensors attached to the gas
123 cell) at the AILES beamline of the SOLEIL synchrotron using a FT spectrometer (Bruker
124 IFS-125HR) associated to a multipass White-type cell with the total optical pathlength
125 $L = 151.75 \pm 1.5$ m. The synchrotron radiation extracted by the AILES beamline of SOLEIL
126 facility (operating in the 500-mA standard multibunch mode) allowed recording absorption
127 spectra in the 50-700 cm^{-1} spectral interval. Additional experiments were performed in the
128 same spectral range with a global source providing much lower power in comparison to the
129 synchrotron radiation. The light intensity transmitted through the absorption cell was
130 measured using a liquid He cooled Si bolometer.

131 The absorption coefficient was determined as $\alpha_{total} = 1/L \ln(I_0(\nu)/I(\nu))$, where $I(\nu)$ and
132 $I_0(\nu)$ correspond to the signal when the cell was filled with the mixture of water vapour and
133 foreign gas (studied spectrum) and with a non-absorbing gas (reference spectrum or baseline),
134 respectively. Typical examples of $I(\nu)$ and $I_0(\nu)$ recordings performed under the same
135 experimental conditions using global and synchrotron sources of far-IR radiation are
136 presented in Fig.1.

137 Prior to the measurements of foreign continuum absorption spectra, recordings
138 with pure N_2 were performed at different pressures to test the baseline stability. They
139 revealed some pressure induced baseline variations, notable for wavenumbers above
140 300 cm^{-1} . These variations are assigned to the deformation of the gas cell windows

141 made of thin film (polypropylene, 50 μm). These changes were almost reproducible
 142 after pumping out and re-filling the cell at the same pressure in the range up to about
 143 400 mbar (presumably due to an elastic deformation of the windows). Higher
 144 pressures resulted in significant and non-reproducible baseline variation (inelastic
 145 deformation). Consequently, the maximum value of the pressure was limited to 400
 146 mbar. More details on the baseline stability tests are provided as *Supplementary*
 147 *Materials* attached to this paper.

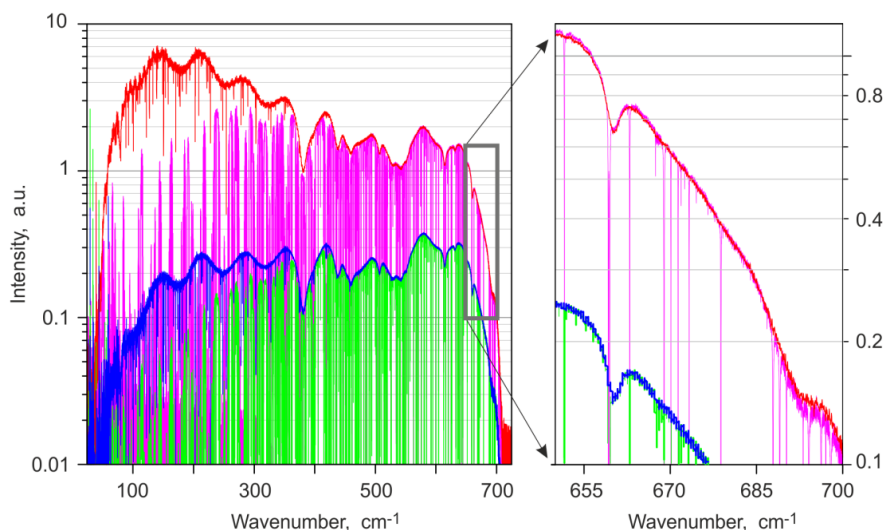


Fig. 1. Typical example of raw FTS spectra for a mixture of 96 mbar of nitrogen and 4 mbar of water vapour (pink) recorded using the synchrotron radiation and corresponding reference spectrum recorded with 100 mbar of pure N₂ (red). Similar recordings with the global source (green and blue, respectively). The zoom on the left panel shows an enlarge portion of the measurements.

148 Five series of spectra were recorded in the experimental conditions summarized in
 149 **Table 1**. The reference spectra providing the baseline were recorded at the beginning of each
 150 series.

Table 1. Experimental conditions.

Foreign gas Gas purity, %	Nitrogen 99.9999			Oxygen 99.9995	Dry air 99.999
Radiation source	global	synchrotron			
Series number	1	2	3	4	5
Number of pressure points	9	10	8	9	8
Filling H ₂ O pressure, mbar	3	2	4	4	4
Min./max. total pressure, mbar	20/100	40/200	100/430	200/400	200/400
Number of acquisitions	200 - 400	200	100 - 200	200	200

151
 152 Each series included two steps. First, the cell was filled with a given pressure of water
 153 vapour and then the foreign gas (N₂, O₂ and dry air for series 1-3, 4 and 5, respectively) was
 154 gradually injected up to the maximum (total) pressure. Spectra were recorded at various
 155 pressure steps of the pressure ramp. Then the gas mixture was pumped out and additional
 156 spectra were recorded for various pressure values during the decreasing pressure ramp. Note
 157 that during the filling with the foreign gas, the partial pressure of water vapour is supposed to
 158 be constant while when the gas mixture is pumped out, the relative concentration of water
 159 vapour is expected to be constant and thus water vapour partial pressure decreases
 160 proportionally to the total pressure.

161 The gas pressure was measured by three complementary sensors (Pfeifer, 10, 100 and
 162 1000 mbar, uncertainty 0.25 % of reading). As mentioned above, for each wet gas spectrum,
 163 the reference spectrum was recorded with the corresponding dry foreign gas at the same
 164 pressure in order to minimize the baseline change. The remaining minor changes of the
 165 baseline (see insert in Fig. 1, near 700 cm⁻¹) were taken into account by introducing an
 166 empirical adjustable parameter as discussed in the next section.

167 Resonance lines due to water vapour present as an impurity are clearly observed in the
 168 reference spectrum (Fig. 1). Corresponding water content was estimated to be less than
 169 0.005 mbar. Such small amount of residual water does not notably impact the resulted
 170 continuum value and can be neglected.

171 The wet (studied) and dry (reference) spectra were recorded with a spectral resolution of
 172 0.02 and 0.2 cm⁻¹, respectively. The resolution of 0.02 cm⁻¹ is comparable to the width of the
 173 resonance lines at the pressure conditions of the recordings; thus as checked in our previous
 174 studies [7-Odintsova2017, 8-Odintsova2019, 9-Odintsova2020], instrumental spectral
 175 function does not notably affect the magnitude of the continuum retrieved between resonance
 176 lines (micro-windows of transparency) and is not taken into account in the data treatment
 177 presented below.

178 3. Data treatment

179 The retrieved absorption coefficient, α_{total} , is considered as the sum of the resonance
 180 lines, α_{res} , and of the continuum absorption, α_{cont} :

$$\alpha_{total}(v, P_{H_2O}, P_{for}) = \alpha_{res}(v, P_{H_2O}, P_{for}) + \alpha_{cont}(v, P_{H_2O}, P_{for}), \quad (1)$$

181 where v is frequency, P_{H_2O} and P_{for} are water vapour and foreign gas partial pressure,
 182 respectively.

183 Resonant absorption was modelled as a line-by-line sum of H₂O lines with the
 184 following profile [23-Clough1989]:

$$\alpha_{Line} = \frac{S}{\pi} R(v) \left(\frac{\Delta v_c}{(v - v_0)^2 + \Delta v_c^2} + \frac{\Delta v_c}{(v + v_0)^2 + \Delta v_c^2} \right), \quad (2)$$

where
$$\Delta v_c = \Delta v_{H_2O} + \Delta v_{for} = P_{H_2O} \cdot \gamma_{H_2O} + P_{for} \cdot \gamma_{for}, \quad (3)$$

and
$$R(v) = \frac{v}{v_0} \frac{\tanh(hv/2kT)}{\tanh(hv_0/2kT)}, \quad (4)$$

185 where Δv_c is the collisional width of the line, γ_{H_2O} and γ_{for} are self- and foreign-gas pressure
 186 broadening coefficients, respectively. Note that the Doppler line width at our experimental
 187 conditions in the frequency range under consideration is less than Δv_c by at least 2 orders of
 188 magnitude and can be neglected. We also neglected the resonance spectrum of O₂ because it
 189 is very weak [24-Tourelle2020] and mostly removed automatically because the reference
 190 spectrum is recorded with dry O₂ at the same pressure. Frequencies (v_0), line strengths (S),
 191 self- and air-broadening coefficients were taken from the HITRAN2016 database [4-
 192 HITRAN2016]. Water lines pressure broadening by nitrogen and oxygen were taken from the
 193 results of calculations [25-Vispoel2019, 26-Gamache2019]. Nitrogen broadening coefficients
 194 were calculated for the three most abundant water isotopologues (H₂¹⁶O, H₂¹⁸O and H₂¹⁷O)
 195 for the transitions in the ground vibrational state Involving values of the total angular
 196 momentum quantum number J lower than 23. In [26-Gamache2019], oxygen broadening
 197 coefficients are provided for the pure rotational transitions of the main isotopologue, H₂¹⁶O,
 198 with $J < 10$. For all other ground state lines we used air-broadening coefficients from

199 HITRAN2016 multiplied by the average (over all lines for which these coefficients are
 200 known) ratio of air- to foreign gas broadening, which was found to be 1.064(57) and 0.67(10)
 201 for N₂- and O₂-broadening, respectively. General consistency between used broadening
 202 parameters was verified assuming that $\gamma_{\text{air}} = 0.79\gamma_{\text{N}_2} + 0.21\gamma_{\text{O}_2}$ (see *Supplementary Materials*
 203 for details). For the other H₂O isotopologues and rotational transitions in vibrationally excited
 204 states, the broadening coefficients were assumed to be the same as for the H₂¹⁶O
 205 corresponding lines in the ground state. [27-Gamache2003, 28-Gamache2004]

206 The standard far-wing cut-off at 25 cm⁻¹ from the line centre was applied, the far wings
 207 of the line below and above the cut-off frequency being excluded and the remaining almost
 208 rectangular absorption (the “pedestal” or “plinth”) underneath the modelled line profile being
 209 preserved as an intrinsic part of the resonance absorption.

210 Total continuum absorption, α_{cont} , was determined by subtracting the calculated
 211 resonance absorption, α_{res} , from the measured absorption coefficient, α_{total} . Considering the
 212 fact that baselines were recorded with the cell filled with the foreign gas at the same pressure
 213 as the one adopted for the wet gas recordings, α_{total} does not include the dry continuum
 214 contribution and is thus the sum of the two wet components, namely self- (α_{self}) and foreign
 215 (α_{for}) -continuum of water vapour:

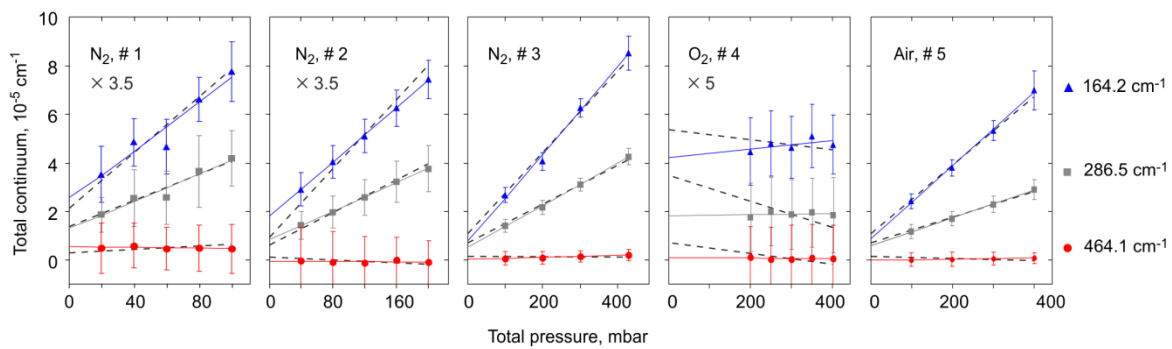
$$\alpha_{\text{cont}}(\nu, P) = \alpha_{\text{self}}(\nu, P) + \alpha_{\text{for}}(\nu, P) = C_s P_{\text{H}_2\text{O}}^2 / kT + C_f P_{\text{H}_2\text{O}} P_{\text{for}} / kT. \quad (5)$$

216 In this formula, C_s and C_f are the self- and foreign-continuum cross-sections (in
 217 cm²molecule⁻¹atm⁻¹), respectively, P is the total pressure of the mixture $P = P_{\text{H}_2\text{O}} + P_{\text{for}}$.

218 The continuum absorption, $\alpha_{\text{cont}}(\nu, P_{\text{H}_2\text{O}}, P_{\text{for}})$, was determined within as many as
 219 possible manually selected micro-windows of transparency between resonance water
 220 lines. Most of the selected micro-windows coincide with those considered in our
 221 previous studies of the self-continuum [8-Odintsova2019, 9-Odintsova2020].

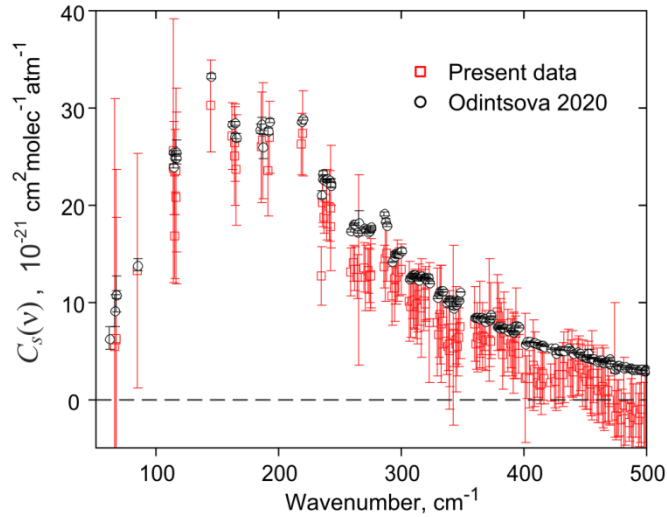
222 **Increasing pressure ramps**

223 During the filling with the foreign gas, the partial pressure of water vapour in the gas is
 224 assumed to be independent of the amount of foreign gas injected in the cell. In this case the
 225 self-continuum absorption remains invariant. The foreign-continuum absorption and thus the
 226 total continuum absorption are expected to increase linearly with the total gas pressure (Eq.
 227 (5)). This is indeed reflected by the obtained pressure dependences (Fig. 2).



228
 229 Fig. 2. Total derived continuum absorption in H₂O-N₂, H₂O-O₂ and H₂O-air mixtures *versus* total
 230 gas pressure for three typical micro-windows during increasing pressure ramps. The absorption
 231 magnitude for Series 1-2 and 4 have been multiplied by 3.5 and 5 respectively. Error bars
 232 correspond to 1 σ standard deviation of the noisy signal from its mean value within the current
 233 micro-window. Solid and dashed straight lines correspond to the best fit of linear function with
 234 and without the empirical correction term $\Delta\alpha$, to the same points (see text for details).
 235

236 The self- and foreign-continuum cross-sections were determined as the fitted values of
 237 the intercept at zero and slope of the foreign gas pressure dependences (Eq. (5)), respectively.
 238 Error bars relative to C_s and C_f were obtained as the statistical errors provided by the fit
 239 weighted according to the uncertainty of each measurement point. The latter corresponds to
 240 one standard deviation of the noisy absorption spectra from its mean value within the current
 241 micro-window. Note that the uncertainties related to measured pressure and temperature
 242 values are negligible. We checked that the self-continuum cross-sections retrieved from
 243 different series of measurement coincide within the 3σ error bars. As illustrated in Fig. 3,
 244 although less accurate, the weighted average values of the five different C_s determinations are
 245 found consistent with the C_s values of [9-Odintsova2020] derived from pure water vapour
 246 spectra. C_f values retrieved from the increasing pressure ramp measurements are provided as
 247 *Supplementary Materials* for the five series. They are considered as preliminary information
 248 which will be validated and discussed in comparison with corresponding values obtained from
 249 decreasing pressure ramps.
 250



251
 252 Fig. 3. Water vapour self-continuum cross-section averaged over all data retrieved in this work
 253 from increasing pressure ramps (open red squares) and similar data from [9-Odintsova2020]
 254 (open black circles). Error bars correspond to 1σ uncertainty.
 255

256 The achieved agreement allows us to use the C_s values of [9-Odintsova2020] to subtract
 257 the calculated self-continuum component from the total measured continuum. In accordance
 258 with Eq. (5), the remaining part is due to the foreign continuum. In these conditions, we
 259 expect a higher accuracy of C_f retrieval by using C_s values of [9-Odintsova2020] in each
 260 experimental series. However, some deviations including quasiperiodic low frequency
 261 variations of the retrieved C_s around the C_s values of [9-Odintsova2020] are notable in Fig. 3.
 262 These deviations, assigned to the remaining baseline variations (see *Supplementary*
 263 *Materials*), can be corrected by introducing an empirical frequency dependent correction
 264 term, $\Delta\alpha(\nu)$, which is used as an adjustable parameter when fitting the model to the
 265 experimental data:
 266

$$267 \alpha_{for}(\nu, P) = \alpha_{cont}(\nu, P) - C_s^{Odintsova} P_{H_2O}^2 / kT = \Delta\alpha(\nu) + C_f P_{H_2O} / kT \quad (6)$$

268

269 Note that the baseline variations, corrected by the introduction of $\Delta\alpha$, may have
 270 different instrumental origins including not only incomplete compensation of the interference
 271 fringes with pressure variations, but other sources such as drift of the mean source power.

272 The impact of $\Delta\alpha$ can be seen in Fig. 2 as a deviation between solid and dashed lines,
 273 the latter corresponding to $\Delta\alpha = 0$. Both lines are well within the uncertainty range of
 274 experimental points but, in average, over all micro-windows the introduction of the correction
 275 term improves the *rms* of the linear fit by a factor of 3. Under the experimental conditions
 276 chosen in this work, the correction term is from about 10 to 100 times smaller than the total
 277 continuum absorption. More details on the correction term magnitude, its impact on the
 278 retrievals of the continuum and its potential relation to the water vapour amount variations are
 279 given in *Supplementary Materials*. Note that $\Delta\alpha(\nu)$ is independent of the pressure and thus C_f
 280 derived at the same time as deriving the C_s from these data (*i.e.* ignoring values of [9-
 281 Odintsova2020]) is the same as deriving it using the formalism of Eq. (6) in the case of the
 282 increasing pressure ramp. However, we introduce the $\Delta\alpha$ correction term at this step because
 283 it is required for the proper data treatment of the decreasing pressure ramps.

284 **Decreasing pressure ramps**

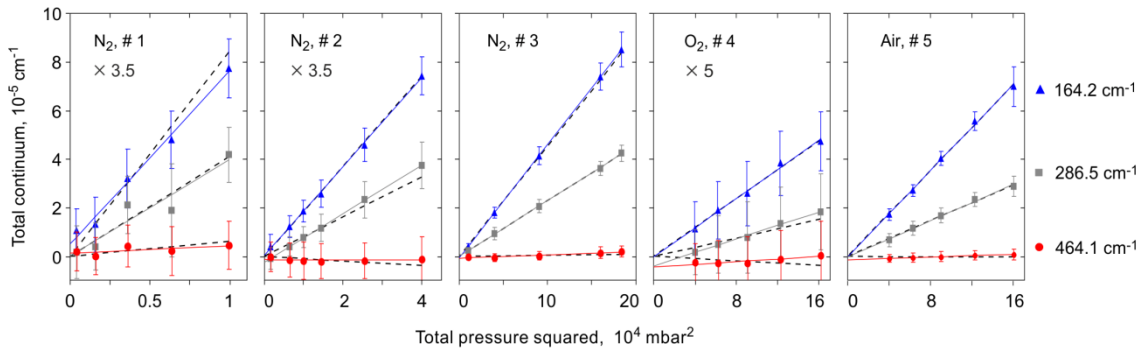
285 The volume fraction (relative concentration) of water vapour in the cell is assumed to be
 286 unchanged during the pumping out of the gas mixture. Thus the P_{H_2O}/P ratio is constant and
 287 Eq. (5) can be modified as follows:

$$288 \alpha_{cont}(\nu, P) = \Delta\alpha(\nu) + \beta(\nu)P^2/kT \quad , \quad (7)$$

289 including the aforementioned adjustable parameter $\Delta\alpha$ corresponding to the remaining
 290 variations of the baseline and

$$291 \beta(\nu) = C_s \left(\frac{P_{H_2O}}{P} \right)^2 + C_f \left(\frac{P_{H_2O}}{P} \right) \left(1 - \frac{P_{H_2O}}{P} \right) \quad (8)$$

292 which is constant within each micro-window. Thus, during the pumping out, the amplitude of
 293 the continuum absorption is expected to decrease proportionally to the total gas pressure
 294 squared. This is indeed confirmed by the experimental results displayed in Fig. 4. Dashed and
 295 solid straight lines are for $\Delta\alpha$ set to zero and variable, respectively. In the latter case, the
 296 deviation of the fit averaged over all micro-windows is improved by a factor of 2.7 (see
 297 *Supplementary Materials* for details).



300 Fig. 4. Total derived continuum absorption in H₂O-N₂, H₂O-O₂ and H₂O-air mixtures *versus* total gas
 301 pressure squared for measurement points in three typical micro-windows at decreasing pressure ramps.
 302 The absorption magnitude for Series 1-2 and 4 have been multiplied by 3.5 and 5 respectively. Error
 303 bars correspond to 1σ standard deviation of the noisy signal from its mean value within the current
 304

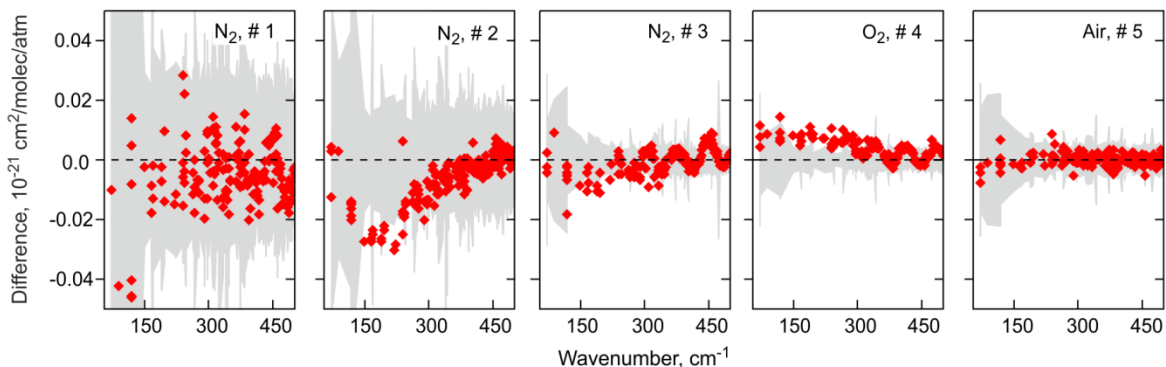
305 micro-window. Solid and dashed straight lines correspond to the best fit with and without the empirical
306 correction term $\Delta\alpha$ (see text for details).

307

308 The foreign-continuum cross-sections were calculated from β values derived from the
309 linear dependence of $\alpha_{cont}(v, P)$ versus P^2 using C_s values from [9-Odintsova2020]. C_f
310 error bars correspond to the statistical uncertainty of the weighted fit of β taking into account
311 the uncertainty of each measurement point. The uncertainty of C_f related to C_s error bar was
312 found to be more than an order of magnitude smaller than the aforementioned statistical
313 uncertainty and was neglected. The uncertainties related to measured pressure and
314 temperature values at this experimental step are also negligible.

315 Figure 5 shows the good agreement between the C_f determinations derived from the
316 increasing and decreasing pressure ramps for all series. The retrieved values coincide within
317 measurement uncertainty, validating the data treatment procedure. Large measurement
318 uncertainty in Series 1 is explained by smaller radiation power available from the global
319 source than from the synchrotron (Fig. 1) and in Series 2 by small amount of water vapour
320 (Table 1), leading in both cases to smaller signal to noise ratio compared to other series.
321 Periodic variations of the difference are seen for Series 3 and 4. **These variations are similar to**
322 **those shown in the lower part of Fig. S1. The similarity indicates an** imperfect elimination of
323 the baseline change by the correction term $\Delta\alpha$. This can be understood as different baselines
324 were used for different pressures, whereas the term takes into account only common
325 variations for all data points.

326



327

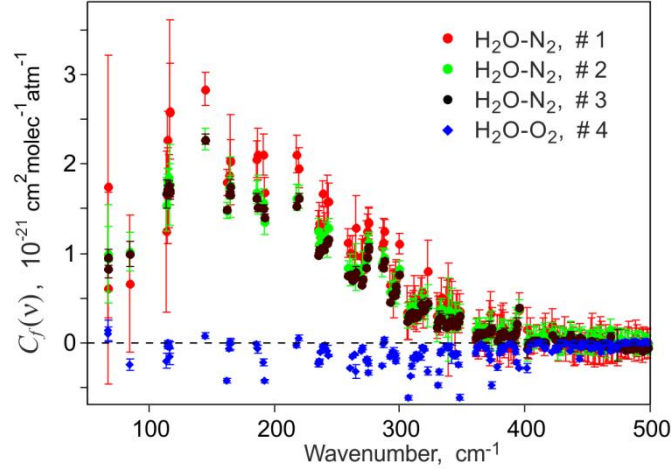
328 Fig. 5. Differences between the retrieved C_f values corresponding to the increasing and decreasing
329 pressure ramps. Grey areas represent $\pm 1\sigma$ joint uncertainty of two datasets centered on zero.

330

331 The C_f values determined from the decreasing pressure ramps are provided as
332 *Supplementary Material*. In the remaining part of the paper we will use mean weighted values
333 from the increasing and decreasing pressure ramps for comparison with literature data.

334 The C_f values related to the H₂O-N₂ continuum were obtained from three experimental
335 series (No. 1-3 in Table 1) performed under different conditions (H₂O relative concentration
336 and radiation sources). The comparison of three series of derived C_f values is displayed in Fig.
337 6. Series 1 corresponding to the global radiation source leads to systematically higher values.
338 Nevertheless, the three sets of data agree within the 3σ measurement uncertainty. The mean
339 weighted values of C_f from all of the three series are provided as *Supplementary Material* as
340 our final derived set of H₂O-N₂ continuum cross-sections. The provided measurement error
341 (evaluated as 68.26% confidence interval) thus includes not only the statistical uncertainty
342 related, for example, to the detector noise in a single spectrum recording, but also a value
343 resulting (in the case of H₂O-N₂ continuum) from the analysis of 27 spectra together with the

344 same number of baselines. So the provided error value takes into account possible systematic
 345 effects related in particular to different gas mixtures, different radiation sources and the
 346 baseline variations due to both pressure drops and/or radiation power drift.



347
 348 Fig. 6. Cross-sections of H₂O-N₂ and H₂O-O₂ foreign-continuum absorption averaged over increasing
 349 and decreasing pressure ramps. Error bars correspond to 1σ combined uncertainty of the two datasets.

350
 351 The H₂O-O₂ continuum turned out to be too weak to be determined in our experimental
 352 conditions (Fig. 6). Only an upper limit of 10⁻²² cm²molec⁻¹atm⁻¹ (to be compared to a
 353 maximum H₂O-N₂ C_f value of about 2×10⁻²¹ cm²molec⁻¹atm⁻¹) can be reported. Large spread
 354 of points and negative cross-sections are due to uncertainties of pressure broadening
 355 parameters (see *Supplementary Materials* for details). This is confirmed by the good
 356 coincidence of the H₂O-O₂ C_f values determined from increasing and decreasing pressure
 357 ramps (Fig. 5). This agreement is several times better than the amplitude of the fluctuations
 358 between successive micro-windows indicating that these fluctuations are mostly due to
 359 inaccuracies in the subtraction of the resonance absorption resulting from an insufficient
 360 knowledge of the pressure broadening coefficients.

361 The H₂O-O₂ continuum results can be used to check the consistency of the H₂O-N₂ and
 362 H₂O-air cross-sections, as discussed in the next section.

364 4. Discussion

365 Water vapour foreign-continuum in the Earth atmosphere is due to molecular collisions of
 366 water molecules with nitrogen (78.084 %), oxygen (20.95 %) and argon (0.934 %):

$$367 \quad \alpha_{H_2O-air} = C_{H_2O-air} P_{H_2O} \frac{P_{air}}{kT} = C_{H_2O-N_2} P_{H_2O} \frac{P_{N_2}}{kT} + C_{H_2O-O_2} P_{H_2O} \frac{P_{O_2}}{kT} + C_{H_2O-Ar} P_{H_2O} \frac{P_{Ar}}{kT}, \quad (9)$$

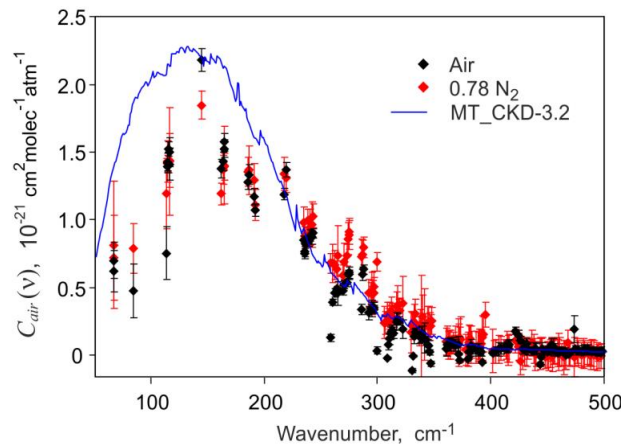
368 where C_{H_2O-air} , $C_{H_2O-N_2}$, $C_{H_2O-O_2}$ and C_{H_2O-Ar} are corresponding foreign-continuum cross-
 369 sections.

370 The contribution of H₂O-Ar pairs to the atmospheric continuum absorption is expected
 371 to be small not only because of the small relative abundance of argon but also because of the
 372 properties of Ar as a collisional partner. For example, the H₂O-Ar cross-section in the
 373 millimetre wavelength range was measured to be several times less than the H₂O-N₂ cross-
 374 section [29-Bauer1998]. We thus consider that the H₂O-Ar contribution to the air absorption

375 continuum is negligible ($C_{H_2O-Ar} = 0$). As shown in the previous section, the H_2O-O_2
 376 continuum was too weak to be determined ($C_{H_2O-O_2} = 0$), which led to the simple relation:

$$C_{H_2O-air} = 0.78C_{H_2O-N_2}. \quad (10)$$

377 **Figure 7** illustrates the good agreement between the measured C_{H_2O-air} values and those
 378 calculated using Eq. (10) and the measured $C_{H_2O-N_2}$ cross-sections. Systematic deviations can
 379 be noted in the range 250-400 cm^{-1} . In our opinion they are related to the inaccuracy of H_2O
 380 line foreign-broadening parameters. The deviations are prominent in this particular range
 381 because the number of micro-windows is increasing towards high frequencies while the
 382 number of intense water lines influencing the continuum magnitude decreases. For further
 383 comparison with literature data (below), our final derived C_{H_2O-air} values corresponding to the
 384 mean weighted from our N_2 and air data, provided as Supplementary Materials, will be used.



385
 386 Fig. 7. H_2O -air (red rhombs) and multiplied by 0.78 H_2O-N_2 (black rhombs) foreign-continuum
 387 cross-sections retrieved in this work. Error bars correspond to 1σ uncertainty. Solid line presents
 388 corresponding data of MT_CKD-3.2 for comparison. Irregular fluctuations of this line are due to
 389 the resonance line pedestals removal from the continuum (see text for details).

390
 391 Before comparing our continuum with previous data, we would like to remind readers
 392 that the continuum magnitude depends directly on the list of resonance lines used to simulate
 393 the monomer absorption (in particular their pressure broadening parameters). For a proper
 394 comparison, the same line list and the same method of resonance absorption calculations
 395 should be used. Considering the number of sources, possible lack of traceability of the used
 396 line parameters, a detailed comparison of C_f data is a tedious work which should be a subject
 397 of a dedicated study. We provide as part of a *Supplementary Material* a discussion of the
 398 possible impact of the used resonance line list to the derived foreign continuum. Thus, the
 399 following comparison should be considered only as a preliminary discussion of the data
 400 obtained in the present work.

401 Three previous laboratory studies can be used for comparison with our results:

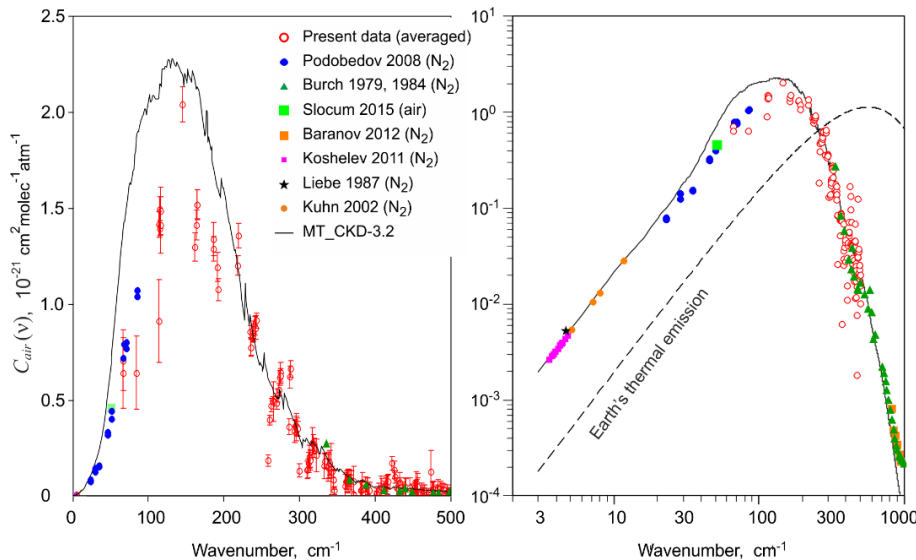
402 (i) The H_2O-N_2 foreign continuum absorption was investigated within 7 micro-windows
 403 in the range of 22-84 cm^{-1} at 293, 313 and 333 K [17-Podobedov2008-N2]. For comparison,
 404 all these data were extrapolated to 296 K using temperature exponent derived in [17-
 405 Podobedov2008-N2] and scaled using Eq. (10). It should be mentioned, that far-wing cut-off

406 at 100 cm^{-1} from the line centre was applied for the resonance absorption model in [17-
 407 [Podobedov2008-N2](#)]. So for comparison with our results, the cumulative contribution of
 408 resonance line wings within the $25\text{-}100\text{ cm}^{-1}$ range of detuning from the line centres were
 409 added to the continuum reported in [17-[Podobedov2008-N2](#)].

410 (ii) Extended series of room temperature measurements of a mixture of water vapour in
 411 air was reported in a narrow interval near 50 cm^{-1} [[30-Slocum2015](#)]. Significant variation of
 412 experimental conditions (optical path length, composition and pressure of the mixture)
 413 allowed quite reliable determination of the H_2O -air continuum.

414 (iii) Finally, Burch performed a systematic experimental study of the H_2O - N_2
 415 continuum in the ranges $338\text{ - }629\text{ cm}^{-1}$ [[19-Burch1979](#)] and $720\text{-}1000\text{ cm}^{-1}$ [[31-Burch_Alt](#)].

416 These previous experimental data and our final derived $C_{\text{H}_2\text{O-air}}$ values are gathered in
 417 [Fig. 8](#) and compared to the MT_CKD-3.2 foreign-continuum model. It should be recalled,
 418 that the MT_CKD continuum includes the "pedestal" (the trapezoid underneath the line
 419 profile subtracted from the resonance absorption) [[11-Mlawer2012](#)]. For the proper
 420 comparison of the experimental data with the MT_CKD model, we subtracted the cumulative
 421 pedestal of the H_2O rotational spectrum from the model spectrum. Note that the latter
 422 modification decreases the model continuum by about 25% in the range of the maximum of
 423 the H_2O band and introduces non-smoothness of the spectrum, which is seen even in
 424 logarithmic scale of the figure. A good overall agreement is obtained with previous
 425 measurements available in the low- and high-frequency wings of the H_2O band. The
 426 agreement with the MT_CKD-3.2 [[13-MTCKD_site](#)] model is very good in the range above
 427 200 cm^{-1} although the model overestimates the continuum in the in-band region ($60\text{-}200\text{ cm}^{-1}$)
 428 where previous measurements were absent.



429
 430
 431 Fig. 8. Comparison of the present results to literature laboratory data on absorption cross-
 432 sections of the H_2O -air continuum at 296 K in linear (left) and logarithmic (right) scales.
 433 Weighted average values of H_2O - N_2 and H_2O -air data from this work (Fig.7) are shown by red
 434 circles. Measurements with H_2O - N_2 mixtures from [[18-Burch1979](#), [31-Burch_Alt](#)] (dark green
 435 triangles) and [[17-Podobedov2008-N2](#)] (blue squares) are multiplied by 0.78 (Eq. (10)). Moist
 436 air measurements from [[29-Slocum2015](#)] are shown by bright green square. Other known
 437 microwave and IR data from [[15-Liebe1987](#), [14-Koshelev2011](#), [16-Kuhn2002](#), [32-Baranov2012](#)]
 438 below and above studied range are shown for comparison by different symbols (see legend in the
 439 figure). The MT_CKD-3.2 model foreign continuum is displayed by black solid curve. The
 440 dotted curve in the right panel is the [Planck's](#) law for the Earth's mean thermal emission
 radiance (in arbitrary units).

441 Note that this overestimation, on one hand, is slightly larger than could be explained by
442 differences in line list, which should be used together with the model [Mlawer2019] for the
443 correct calculation of the total absorption in air but, on the other hand, it is well within the
444 limits of C_f variation related to water line pressure broadening parameter uncertainties (see
445 *Supplementary Materials* for details).

446 The results of other known laboratory studies related to the H₂O-air foreign continuum
447 are presented in Fig. 8 including **datasets** retrieved at lower and higher frequencies than our
448 work. Additionally, we plotted in the figure the black-body spectral radiance curve (Planck's
449 law) for a temperature 287 K corresponding to the mean thermal emission of the Earth and
450 demonstrating the importance of the considered spectral range for the radiation budget of our
451 planet. As the maximum of the thermal emission curve is close to the range of the H₂O-air
452 continuum maximum, the continuum uncertainty directly **affects** the corresponding
453 uncertainty of the outgoing energy.

454 **5. Conclusion**

455 The foreign-continuum absorption of moist nitrogen, oxygen and air has been
456 investigated using synchrotron-based Fourier transform spectroscopy at room temperature in
457 the 50-500 cm⁻¹ frequency range. Cross-section values were derived from the pressure
458 dependence of the measured absorption for series of pressure values during increasing and
459 decreasing pressure ramps. The oxygen contribution to the foreign continuum of water vapour
460 in air is found to be mostly negligible compared to the N₂ contribution. The foreign
461 continuum in air is thus limited to the N₂ contribution and a good consistency is obtained
462 between the results obtained with air and with N₂.

463 To the best of our knowledge, the reported results are the first laboratory study of water
464 vapour foreign-continuum covering the entire spectral range of the H₂O rotational band. Our
465 data on the water vapour foreign-continuum are consistent with earlier experimental results of
466 Podobedov [17-Podobedov2008_N2] and Burch [19-Burch1979] in the lower and upper parts
467 of the studied spectral range, respectively, and in general confirm the validity of the
468 MT_CKD model widely used for atmospheric applications.

469

470 **Acknowledgements**

471 This work became possible thanks to the Project No. 20180347 supported by SOLEIL
472 Synchrotron Team. Experimental part of the work was performed under partial financial
473 support from the RFBR research project No. 18-55-16006. Resonance absorption modelling
474 and continuum data analysis were funded by RFBR within the research projects No. 18-02-
475 00705 and No. 18-05-00698, respectively.

476

477 **Credit author statement**

478 A.O. Koroleva: Formal analysis; Methodology; Writing - original draft

479 T.A. Odintsova: Data curation; Investigation; Methodology

480 M.Yu. Tretyakov: Conceptualization, Data curation, Writing - review & editing

481 O. Pirali: Data curation; Resources; Methodology

482 A. Campargue: Formal analysis; Validation; Writing - review & editing

483

References

484

485 [1-Clough1992] Clough SA, Iacono MJ, Moncet J.-L. Line-by-line calculations of atmospheric
486 fluxes and cooling rates: Application to water vapour. *J Geophys Res* 1992;97/D14:15761-85.

487 [2-Harries2000] Harries JE. Physics of the Earth's radiative energy balance. *Contemp Phys*
488 2000;41/5:309-22. DOI: 10.1080/001075100750012803.

489 [3-Shine2012] Shine KP, Ptashnik IV, Rädel G. The water vapour continuum: brief history and
490 recent developments. *Surv Geophys* 2012;33:535–55. DOI 10.1007/s10712-011-9170-y

491 [4-HITRAN2016] Gordon IE, Rothman LS, Hill C, Kochanov RV, Tan Y, Bernath PF, et al. The
492 HITRAN2016 molecular spectroscopic database. *J Quant Spectrosc Radiat Transfer* 2017;203:3–
493 69.

494 [5-Boissoles2003] Boissoles J, Boulet C, Tipping RH, Brown A, Ma Q. Theoretical calculation of
495 the translation-rotation collision-induced absorption in N₂-N₂, O₂-O₂, and N₂-O₂ pairs. *J Quant*
496 *Spectrosc Radiat Transfer* 2003;82:505–16.

497 [6-Consolino2017] Consolino L, Bartalini S, De Natale P. Terahertz frequency metrology for
498 spectroscopic applications: a review. *J Infrared Milli Terahz Waves* 2017;38:1289–315. DOI
499 10.1007/s10762-017-0406-x

500 [7-Odintsova2017] Odintsova TA, Tretyakov MYu, Pirali O, Roy P. Water vapour continuum in
501 the range of rotational spectrum of H₂O molecule: new experimental data and their comparative
502 analysis. *J Quant Spectrosc Radiat Transfer* 2017;187:116–23.

503 [8-Odintsova2019] Odintsova TA, Tretyakov MYu, Zibarova AO, Pirali O, Roy P, Campargue A.
504 Far-infrared self-continuum absorption of H₂¹⁶O and H₂¹⁸O (15–500 cm⁻¹). *J Quant Spectrosc*
505 *Radiat Transfer* 2019;227:190–200.

506 [9-Odintsova2020] Odintsova TA, Tretyakov MYu, Simonova AA, Ptashnik IV, Pirali O,
507 Campargue A. Measurement and temperature dependence of the water vapour self-continuum
508 between 70 and 700 cm⁻¹. *J Mol Struct* 2020;1210:128046. DOI 10.1016/j.molstruc.2020.128046

509 [10-Burch1982] Burch DE. 1982. Continuum absorption by H₂O. Report No AFGL-TR-81-
510 03001982.

511 [11-Mlawer2012] Mlawer EJ, Payne VH, Moncet JL, Delamere JS, Alvarado MJ, Tobin DC.
512 Development and recent evaluation of the MT_CKD model of continuum absorption. *Phil Trans R*
513 *Soc A* 2012;370:2520–56.

514 [12-Mlawer2019] Mlawer EJ, Turner DD, Paine SN, Palchetti L, Bianchini G, Payne VH,
515 Cady - Pereira KE, Pernak RL, Alvarado MJ, Gombos D, Delamere JS, Mlynczak MG, Mast JC.
516 Analysis of water vapour absorption in the far - infrared and submillimeter regions using surface
517 radiometric measurements from extremely dry locations. *J Geophys Res-Atmos*
518 2019;124(14):8134-60.

- 519 [13-MTCKD_site] <https://doi.org/10.1098/rsta.2011.0295.>; Continuum model, (n.d.)
520 http://rtweb.aer.com/continuum_frame.html (accessed December 15, 2020)]
- 521 [14-Koshelev2011] Koshelev MA, Serov EA, Parshin VV, Tretyakov MYu. Millimeter Wave
522 Continuum Absorption in Moist Nitrogen at Temperatures 261–328 K. *J Quant Spectrosc Radiat*
523 *Transfer* 2011;112:2704-12.
- 524 [15-Liebe1987] Liebe HJ, Layton DH. Millimeter-wave properties of the atmosphere: laboratory
525 studies and propagation modeling. NTIA Report. No. 87-224; 1987.
- 526 [16-Kuhn2002] Kuhn T, Bauer A, Godon M, Buehler S, Kuenzi K. Water vapour continuum:
527 absorption measurements at 350 GHz and model calculations. *J Quant Spectrosc Radiat Transfer*
528 2002;74:545–62.
- 529 [17-Podobedov2008-N2] Podobedov VB, Plusquellic DF, Siegrist KE, Fraser GT, Ma Q, Tipping
530 RH. New measurements of the water vapour continuum in the region from 0.3 to 2.7 THz. *J Quant*
531 *Spectrosc Radiat Transfer* 2008;109:458–67.
- 532 [18-Podobedov2008-O2] Podobedov VB, Plusquellic DF, Siegrist KE, Fraser GT, Ma Q, Tipping
533 RH. Continuum and magnetic dipole absorption of the water vapour—oxygen mixtures from 0.3
534 to 3.6 THz. *J Quant Spectrosc Radiat Transfer* 2008;251:203–9
- 535 [19-Burch1979] Burch D.E., Gryvnak D.A. 1979 Method of calculating H₂O transmitting between
536 333 and 633 cm⁻¹. Report No AFGL-TR-79-0054
- 537 [20-Green2012] Green PD, Newman SM, Beeby RJ, Murray J E, Pickering JC, Harries J E.
538 Recent advances in measurement of the water vapour continuum in the far- infrared spectral
539 region. *Philosophical Transactions. Series A, Mathematical, Physical, and*
540 *Engineering Sciences* 2012;370(1968);2637–55. <https://doi.org/10.1098/rsta.2011.0263>
- 541 [21-Liuzzi2014] Liuzzi G, Masiello G, Serio C, Palchetti L, Bianchini G. Validation of water
542 vapour continuum absorption models in the wave number range 180–600 cm⁻¹ with atmospheric
543 emitted spectral radiance measured at the Antarctica Dome- C site. *Optics Express*
544 2014;22(14);16784–801. doi:10.1364/OE.22.016784
- 545 [22-Shi2016] Shi S-C, Paine S, Yao QJ, Lin ZH, Li XX, Duan WY, et al. Terahertz and far-
546 infrared windows opened at Dome A in Antarctica. *Nature Astronomy* 2016;1(1);1–7.
547 <https://doi.org/10.1038/s41550-016-0001>
- 548 [23-Clough1989] Clough SA, Kneizys FX, Davies RW. Line shape and water vapor continuum.
549 *Atospheric Research* 1989;23:229-41.
- 550 [24-Touaille2020] Touaille M, Béguier S, Odintsova TA, Tretyakov MYu, Pirali O, Campargue
551 A. The O₂ far-infrared absorption spectrum between 50 and 170 cm⁻¹. *J Quant Spectrosc Radiat*
552 *Transfer* 2020;242:106709. doi.org//10.1016/j.jqsrt.2019.106709
- 553 [25-Vispoel2019] Vispoel B, Cavalcanti JH, Gamache RR. Modified complex Robert-Bonamy
554 calculations of line shape parameters and their temperature dependence for water vapour in
555 collision with N₂. *J Quant Spectrosc Radiat Transfer* 2019;228:79–89.
- 556 [26-Gamache2019] Gamache R. Private communication, 2019.

- 557 [27-Gamache2003] Gamache RR, Fischer J. Half-widths of H₂¹⁶O, H₂¹⁸O, H₂¹⁷O, HD¹⁶O, and
558 D₂¹⁶O: I. Comparison between isotopomers. *J Quant Spectrosc Radiat Transfer* 2003;78:289–304.
- 559 [28-Gamache2004] Gamache RR, Hartmann J-M. Collisional parameters of H₂O lines: effects of
560 vibration. *J Quant Spectrosc Radiat Transfer* 2004;83:119–47.
- 561 [29-Bauer1998] Bauer A, Godon M, Carlier J, Gamache RR. Continuum in the windows of the
562 water vapour spectrum. Absorption of H₂O-Ar at 239 GHz and linewidth calculations. *J Quant
563 Spectrosc Radiat Transfer* 1998;59(3-5):273-85.
- 564 [30-Slocum2015] Slocum DM, Giles RH, Goyette TM. High-resolution water vapour spectrum
565 and line shape analysis in the terahertz region. *J Quant Spectrosc Radiat Transfer* 2015;159:69–79.
- 566 [31-Burch_Alt] Burch DE, Alt RL. 1984 Continuum absorption by H₂O in the 700–1200 cm⁻¹ and
567 2400–2800 cm⁻¹ windows. US Air Force Geophysics Laboratory report AFGL-TR-84-0128,
568 Hanscom Air Force Base, MA, USA.
- 569 [32-Baranov2012] Baranov YuI, Lafferty WJ. The water vapour self- and water–nitrogen
570 continuum absorption in the 1000 and 2500 cm⁻¹ atmospheric windows. *Phil. Trans. R. Soc. A.*
571 2012; 370: 2578–2589
- 572

The authors declare that they have no known competing financial interests or personal relationships that could have appeared to influence the work reported in this paper.

Credit author statement

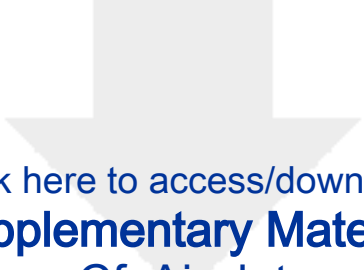
A.O. Koroleva: Formal analysis; Methodology; Writing - original draft

T.A. Odintsova: Data curation; Investigation; Methodology

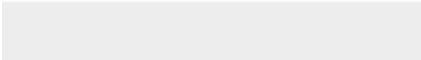
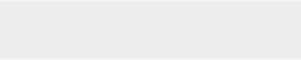
M.Yu. Tretyakov: Conceptualization, Data curation, Writing - review & editing

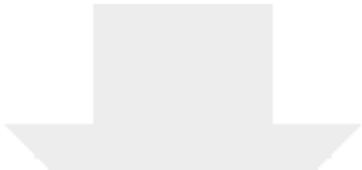
O. Pirali: Data curation; Resources; Methodology

A. Campargue: Formal analysis; Validation; Writing - review & editing



Click here to access/download
Supplementary Material
Cf_Air.dat



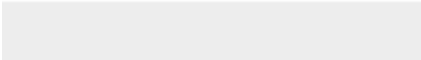
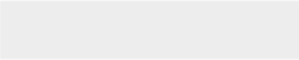


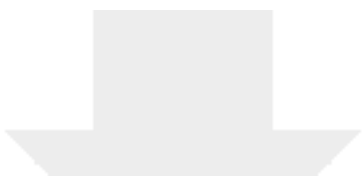
Click here to access/download
Supplementary Material
Cf_N2.dat





Click here to access/download
Supplementary Material
Cf_O2.dat





Click here to access/download
Supplementary Material
Cs.dat





Click here to access/download
Supplementary Material
SupMat_rev2.pdf

